

Segmentation of Polarimetric SAR images based on the SIRV model and the Kummeru PDF.

Lionel BOMBRUN, Gabriel VASILE, Michel GAY

Grenoble Image Parole Signal et Automatique (GIPSA-lab)

CNRS INPG - 961, Rue de la Houille Blanche, BP 46, 38402 Saint-Martin-d'Hères, France

lionel.bombrun@gipsa-lab.grenoble-inp.fr, gabriel.vasile@gipsa-lab.grenoble-inp.fr,
michel.gay@gipsa-lab.grenoble-inp.fr

Résumé – Dans le contexte des modèles de fouillis polarimétriques non gaussien, ce papier présente une application des récentes avancées dans le domaine des processus sphériquement invariants (SIRV) pour la l'estimation de la matrice de cohérence dans des zones de fouillis hétérogène. Les données polarimétriques radar sont décrites complètement à travers deux paramètres indépendants : le span et la matrice de cohérence normalisée. La matrice de cohérence normalisée décrit l'information polarimétrique tandis que le span montre la puissance rétrodiffusée. À l'aide du modèle SIRV, une nouvelle distance au sens du maximum de vraisemblance est introduite pour segmenter les images polarimétriques. La méthode proposée est ensuite testée sur une image acquise par le système aéroporté RAMSES.

Abstract – In the context of non-Gaussian polarimetric clutter models, this paper presents an application of the recent advances in the field of Spherically Invariant Random Vectors (SIRV) modelling for coherency matrix estimation in heterogeneous clutter. The complete description of the POLSAR data set is achieved by estimating the span and the normalized coherency independently. The normalized coherency describes the polarimetric diversity, while the span indicates the total received power. Based on the SIRV model, a new maximum likelihood distance measure is introduced for unsupervised POLSAR segmentation. The proposed method is tested with airborne POLSAR images provided by the RAMSES system.

1 Introduction

In a particular frequency band, the wave-media interactions over distributed areas are generally studied using the polarimetric covariance matrix. In general, POLSAR data are locally modelled by the multivariate, zero mean, circular Gaussian probability density function, which is completely determined by the covariance matrix.

The recently launched POLSAR systems are now capable of producing high quality images of the Earth's surface with meter resolution. The decrease of the resolution cell offers the opportunity to observe much thinner spatial features than the decametric resolution of the up-to-now available SAR images. Recent studies [4] show that the higher scene heterogeneity leads to non-Gaussian polarimetric clutter modelling, especially for urban areas.

This paper presented a new estimation scheme for deriving normalized coherency matrices and the resulting estimated span with high resolution POLSAR images. The proposed Fixed Point estimator is independent on the span Probability Density Function (PDF) and represents an approximate ML estimator for a large class of stochastic processes obeying the SIRV model. Here, we propose to use the Fisher PDF to model the estimated texture parameter. For a Fisher distributed texture, authors prove that the target scattering vector k follows a Kummeru PDF. For SIRV clutter, a new approximate ML distance

measure is introduced for unsupervised POLSAR classification. The effectiveness of the proposed estimation/segmentation scheme is illustrated by very high resolution X-band POLSAR data.

2 SIRV model

2.1 Definition

With the new generation of airborne and spaceborne SAR sensors, the number of scatterers present in each resolution cell decreases considerably, homogeneous hypothesis of the POLSAR clutter can be reconsidered. Heterogeneous clutter models have therefore recently been studied.

In 1973, Kung Yao has first introduced the use of SIRV and their applications to estimation and detection in communication [10]. From a PolSAR point of view, the target vector \mathbf{k} is defined as the product of a square root of a positive random variable τ (representing the texture) with an independent complex Gaussian vector \mathbf{z} with zero mean and covariance matrix $[M] = E\{\mathbf{z}\mathbf{z}^H\}$ (representing the speckle) :

$$\mathbf{k} = \sqrt{\tau} \mathbf{z} \quad (1)$$

where the superscript H denotes the complex conjugate transposition and $E\{\cdot\}$ the mathematical expectation.

For a given covariance matrix $[M]$, the ML estimator of the texture parameter τ is given by :

$$\hat{\tau}_i = \frac{\mathbf{k}_i^H [M]^{-1} \mathbf{k}_i}{p} \quad (2)$$

where p is the dimension of the target scattering vector \mathbf{k} ($p = 3$ for the reciprocal case).

The ML estimator of the normalized covariance matrix under the deterministic texture case is the solution of the following recursive equation :

$$[\hat{M}]_{FP} = f([\hat{M}]_{FP}) = \frac{p}{N} \sum_{i=1}^N \frac{\mathbf{k}_i \mathbf{k}_i^H}{\mathbf{k}_i^H [\hat{M}]_{FP}^{-1} \mathbf{k}_i} \quad (3)$$

Pascal et al. have established the existence and the uniqueness, up to a scalar factor, of the Fixed Point estimator of the normalized covariance matrix, as well as the convergence of the recursive algorithm whatever the initialization [7] [8]. In this paper, the trace of the covariance matrix is normalized to p the dimension of target scattering vector.

It is important to notice that in the SIRV definition, the PDF of the texture random variable is not explicitly specified. As a consequence, SIRVs describe a whole class of stochastic processes. This class includes the conventional clutter models having Gaussian, \mathcal{K} -distributed, Rayleigh or Weibull PDFs.

2.2 Texture modeling

2.2.1 Definition

The texture parameter τ is the random power of the clutter, it characterizes the randomness induced by variations in the radar backscattering over different polarization channels. This texture parameter can be rewritten as the product of a normalized texture parameter ξ with the mean backscattered power μ by :

$$\tau = \mu \xi \quad (4)$$

For a segment S containing N pixels, the normalized texture parameter for pixel i is defined by :

$$\xi_i = \frac{\tau_i}{\mu} = \frac{\tau_i}{\frac{1}{N} \sum_{j=1}^N \tau_j} = \frac{\mathbf{k}_i^H [M]^{-1} \mathbf{k}_i}{\frac{1}{N} \sum_{j=1}^N \mathbf{k}_j^H [M]^{-1} \mathbf{k}_j} \quad (5)$$

A common assumption is to consider τ and μ as two chi-squared random variable with respectively ν_1 and ν_2 degrees of freedom. Hence, if τ and μ are independent, ξ follows a Beta Prime distribution with ν_1 and ν_2 parameters. In practice, τ and μ are not independent, but it is reasonable to assume that ξ follows a Beta Prime distribution with other parameters (\mathcal{L} and \mathcal{M}).

2.2.2 Beta Prime PDF

Let ξ be a positive random variable distributed according to a Beta Prime distribution. Its PDF is defined by two parameters \mathcal{L} and \mathcal{M} as :

$$\mathcal{BP}[\xi|\mathcal{L}, \mathcal{M}] = \frac{\Gamma(\mathcal{L} + \mathcal{M})}{\Gamma(\mathcal{L})\Gamma(\mathcal{M})} \frac{\xi^{\mathcal{L}-1}}{(1 + \xi)^{\mathcal{L}+\mathcal{M}}} \quad (6)$$

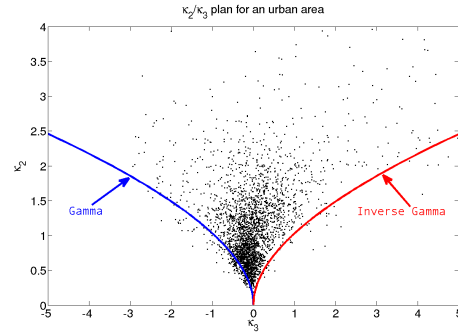


FIG. 1 – κ_2/κ_3 plan for an urban area over the Oberpfaffenhofen test-site (ESAR, L-band).

If ξ follows a Beta Prime PDF with \mathcal{L} and \mathcal{M} parameters, the texture parameter τ is Fisher distributed with $m = \frac{\mu\mathcal{L}}{\mathcal{M}}$, \mathcal{L} and \mathcal{M} parameters.

2.2.3 Fisher PDF

The Fisher distribution is the Pearson type VI distribution. Its PDF is defined by three parameters m , $\mathcal{L} > 0$ and $\mathcal{M} > 0$ as the Mellin convolution of a Gamma PDF by an Inverse Gamma PDF by [6] :

$$\begin{aligned} \mathcal{F}[\tau|m, \mathcal{L}, \mathcal{M}] &= \mathcal{G}[m, \mathcal{L}] \hat{\star} \mathcal{GI}[1, \mathcal{M}] \\ &= \frac{\Gamma(\mathcal{L} + \mathcal{M})}{\Gamma(\mathcal{L})\Gamma(\mathcal{M})} \frac{\mathcal{L}}{\mathcal{M}m} \frac{\left(\frac{\mathcal{L}\tau}{\mathcal{M}m}\right)^{\mathcal{L}-1}}{\left(1 + \frac{\mathcal{L}\tau}{\mathcal{M}m}\right)^{\mathcal{L}+\mathcal{M}}} \end{aligned} \quad (7)$$

2.2.4 Benefit of Fisher PDF

An urban area (80×35 pixels) from the L-band ESAR data over the Oberpfaffenhofen test-site has been extracted. Then, the covariance matrix $[M]_{FP}$ and the texture parameter τ are estimated according to Eq.2 and Eq. 3. To see the benefit of Fisher PDF to model PolSAR clutter, the κ_2/κ_3 plan has been plotted on Fig. 1. It shows the evolution of the second log-cumulant versus the third log-cumulant. In this plan, Gamma and Inverse Gamma PDF are respectively represented by the blue and red line. Fisher PDF cover all the space between the blue and red line.

This example shows that Fisher PDF are well adapted to model high resolution PolSAR clutter.

2.3 Target scattering PDF for a Fisher distributed clutter

The PDF of the target scattering vector can be expressed with the density generator function $h_p(\mathbf{k}^H [M]^{-1} \mathbf{k})$ by [3] :

$$p_{\mathbf{k}}(\mathbf{k}|[M], \mathcal{L}, \mathcal{M}, m) = \frac{1}{\pi^p |[M]|} h_p(\mathbf{k}^H [M]^{-1} \mathbf{k}) \quad (8)$$

where, for a Fisher distributed clutter, the density generator function $h_p(\cdot)$ is defined by [1] :

$$h_p(\mathbf{k}^H [M]^{-1} \mathbf{k}) = \frac{\Gamma(\mathcal{L} + \mathcal{M})}{\Gamma(\mathcal{L})\Gamma(\mathcal{M})} \left(\frac{\mathcal{L}}{\mathcal{M}m} \right)^p \Gamma(p + \mathcal{M}) U(a; b; z) \quad (9)$$

with $a = p + \mathcal{M}$, $b = 1 + p - \mathcal{L}$ and $z = \frac{\mathcal{L}}{\mathcal{M}m} \mathbf{k}^H [M]^{-1} \mathbf{k}$.

$|\cdot|$ and $U(\cdot; \cdot; \cdot)$ denotes respectively the determinant operator and the confluent hypergeometric function of the second kind (KummerU). This PDF has been named the KummerU PDF.

2.4 Maximum Likelihood (ML) estimator

If the density generator function can be mathematically established, the exact ML estimator of the normalized covariance matrix is the solution of the following recursive equation :

$$[\hat{M}_{ML}] = \frac{1}{N} \sum_{i=1}^N \frac{h_{p+1}(\mathbf{k}_i^H [\hat{M}_{ML}]^{-1} \mathbf{k}_i)}{h_p(\mathbf{k}_i^H [\hat{M}_{ML}]^{-1} \mathbf{k}_i)} \mathbf{k}_i \mathbf{k}_i^H \quad (10)$$

Chitour and Pascal have proved that Eq. 10 admits a unique solution and that its corresponding iterative algorithm converges to the Fixed Point solution for every admissible initial condition [2]. In practice, the algorithm is initialized with the identity matrix $[I_p]$.

For a Fisher distributed clutter, the density generator function has been obtained in Eq. 9. The exact ML estimator of the normalized covariance matrix exists. One can replace the density generator function by its expression in Eq. 10. It yields :

$$[\hat{M}_{ML}] = \frac{p + \mathcal{M}}{N} \left(\frac{\mathcal{L}}{\mathcal{M}m} \right) \times \sum_{i=1}^N \frac{U\left(p + 1 + \mathcal{M}; 2 + p - \mathcal{L}; \frac{\mathcal{L}}{\mathcal{M}m} \mathbf{k}_i^H [\hat{M}_{ML}]^{-1} \mathbf{k}_i\right)}{U\left(p + \mathcal{M}; 1 + p - \mathcal{L}; \frac{\mathcal{L}}{\mathcal{M}m} \mathbf{k}_i^H [\hat{M}_{ML}]^{-1} \mathbf{k}_i\right)} \mathbf{k}_i \mathbf{k}_i^H \quad (11)$$

3 Optimal GLRT segmentation

In this section, we propose to implement the SIRV estimation scheme and the KummerU PDF presented in section 2 to segment PolSAR data. This segmentation is based on the Generalized Likelihood Ratio Test formalism.

3.1 Multiple composite hypothesis test

We consider the POLSAR segmentation as the following multiple composite hypothesis test :

$$\begin{cases} H_0 : \mathbf{k} = \sqrt{\tau} \mathbf{z}, \text{ with } \tau \sim \mathcal{F}[m, \mathcal{L}, \mathcal{M}] \text{ and } \mathbf{z} \sim \mathcal{N}[\mathbf{0}, [M]] \\ H_1 : \mathbf{k} = \sqrt{\tau} \mathbf{z}, \text{ with } \tau \sim \mathcal{F}[m_1, \mathcal{L}_1, \mathcal{M}_1] \text{ and } \mathbf{z} \sim \mathcal{N}[\mathbf{0}, [M_1]] \\ \vdots \\ H_C : \mathbf{k} = \sqrt{\tau} \mathbf{z}, \text{ with } \tau \sim \mathcal{F}[m_C, \mathcal{L}_C, \mathcal{M}_C] \text{ and } \mathbf{z} \sim \mathcal{N}[\mathbf{0}, [M_C]] \end{cases} \quad (12)$$

where \mathcal{C} is the number of segments. m , \mathcal{L} and \mathcal{M} are the Fisher parameters and $[M]$ is the normalized covariance matrix of the observed independent identically distributed N secondary data. Notice that the segmentation in \mathcal{C} segments is equivalent to testing $\mathcal{C} + 1$ hypotheses.

In this paper we suppose that the multiple hypotheses from Eq. 12 are not nested, i.e. there is a unique set of parameters (m , \mathcal{L} , \mathcal{M} and $[M]$) characterizing each class. This implies that each class is described by a different SIRV, and hence the extended GLRT can be applied.

3.2 GLRT similarity measure

In multiple composite hypothesis test, the likelihood ratios are sufficient for optimal segmentation problem. The use of likelihood ratios referenced to a "dummy" hypothesis has been introduced in [9]. In consequence, the secondary data observed at instance $t + 1$ are assigned to the segment ω , which maximizes the extended GLRT over all classes characterized by their normalized covariance matrices and Fisher parameters estimated at instance t :

$$\begin{aligned} \omega &= \underset{1 \leq i \leq \mathcal{C}}{\text{Argmax}} \Lambda_i = \underset{1 \leq i \leq \mathcal{C}}{\text{Argmax}} \frac{p_{\mathbf{k}}(\mathbf{k}_1, \dots, \mathbf{k}_N | H_i)}{p_{\mathbf{k}}(\mathbf{k}_1, \dots, \mathbf{k}_N | H_0)} \\ &= \underset{1 \leq i \leq \mathcal{C}}{\text{Argmax}} \frac{\prod_{a=1}^N p_{\mathbf{k}}(\mathbf{k}_a | H_i)}{\prod_{b=1}^N p_{\mathbf{k}}(\mathbf{k}_b | H_0)} \end{aligned} \quad (13)$$

where $p_{\mathbf{k}}(\mathbf{k}_1, \dots, \mathbf{k}_N | H_i)$ is the PDF under the H_i hypothesis.

By taking the natural logarithm of Eq. 13, one can prove that, for a Fisher distributed clutter, Eq. 13 is equivalent to :

$$\begin{aligned} \omega &= \underset{1 \leq i \leq \mathcal{C}}{\text{Argmin}} \ln \left(\frac{|[\hat{M}_i]_{ML}|}{|[\hat{M}]_{ML}|} \right) + \ln \left(\frac{\Gamma(\hat{\mathcal{L}}_i) \Gamma(\hat{\mathcal{M}}_i)}{\Gamma(\hat{\mathcal{L}}_i + \hat{\mathcal{M}}_i)} \right) \\ &+ \ln \left(\frac{\Gamma(\hat{\mathcal{L}} + \hat{\mathcal{M}})}{\Gamma(\hat{\mathcal{L}}) \Gamma(\hat{\mathcal{M}})} \right) + p \ln \left(\frac{\hat{\mathcal{L}}}{\hat{\mathcal{M}} \hat{m}_i} \frac{\hat{\mathcal{M}}_i \hat{m}_i}{\hat{\mathcal{L}}_i} \right) + \ln \left(\frac{\Gamma(p + \hat{\mathcal{M}})}{\Gamma(p + \hat{\mathcal{M}}_i)} \right) \\ &- \frac{1}{N} \sum_{a=1}^N \ln \left\{ U \left(p + \hat{\mathcal{M}}_i; 1 + p - \hat{\mathcal{L}}_i; \frac{\hat{\mathcal{L}}_i}{\hat{\mathcal{M}}_i \hat{m}_i} \mathbf{k}_a^H [M_i]_{ML}^{-1} \mathbf{k}_a \right) \right\} \\ &+ \frac{1}{N} \sum_{b=1}^N \ln \left\{ U \left(p + \hat{\mathcal{M}}; 1 + p - \hat{\mathcal{L}}; \frac{\hat{\mathcal{L}}}{\hat{\mathcal{M}} \hat{m}} \mathbf{k}_b^H [\hat{M}]_{ML}^{-1} \mathbf{k}_b \right) \right\} \end{aligned} \quad (14)$$

where $\hat{\mathcal{L}}_i$, $\hat{\mathcal{M}}_i$, \hat{m}_i and $[\hat{M}_i]_{ML}$ at instance t are respectively the ML estimates of \mathcal{L}_i , \mathcal{M}_i , m_i and $[M_i]_{ML}$ for the segment i at instance $t - 1$ (Eq. 10).

4 Segmentation results

4.1 On synthetic data

To construct the data-set, four 100×100 Gaussian realizations (speckle) are generated. Then, the speckle is multiplied with a texture image containing Fisher realizations. The same Fisher PDF is used in the whole image. Fig. 2(a) shows a colored composition in the Pauli basis of the target scattering

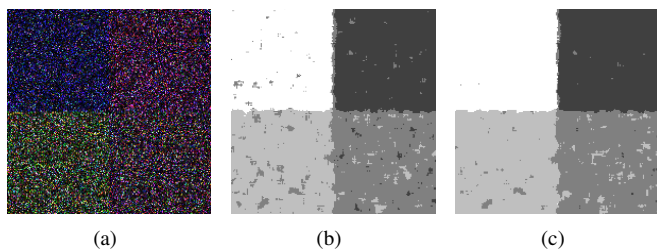


FIG. 2 – Classification results of a simulated data-set (200×200 pixels) : (a) Colored composition of the target vector $[k]_1-[k]_3-[k]_2$, (b) SIRV criterion, (c) KummerU criterion

vector (200×200 pixels). Segmentation results based on the SIRV and KummerU criterion (Eq. 14) are respectively shown on Fig. 2(b) and Fig. 2(c). To evaluate the performances, the confusion matrix for the SIRV and KummerU classifier are computed on Tab. 1.

TAB. 1 – Confusion matrix for the SIRV and KummerU classifier.

97.32	0	2.68	0	98.59	1.39	0	0.0213
0	91.25	8.62	0.13	0.81	92.42	6.77	0
2.93	5.10	91.97	0	0	3.80	95.95	0.24
0.04	1.61	2.48	95.87	0.04	0.90	0.45	98.61

4.2 On very high resolution PolSAR data

Here, the proposed classifier is applied on a very high resolution PolSAR image. This data-set has been acquired by the X-band RAMSES airborne sensor with a resolution of 0.57m. Fig. 3(a) shows a colored composition in the Pauli basis of target scattering vector. Classification results shown on Fig. 3(b), Fig. 3(c) and 3(d) are respectively done with the Wishart, SIRV and KummerU criterion. Each algorithms are first initialized with a partition obtained by the H/α plan. H and α represent respectively the entropy and the mean scattering angle [5].

5 Conclusion

In this paper, authors have proposed to implement the SIRV estimation scheme to derive the normalized covariance matrix and the texture parameter. Based on some statistical consideration, the Beta Prime PDF has been introduced to describe the normalized texture component, which implies a Fisher distributed texture. Then, this statistical scalar model has been successfully validated to characterize high resolution urban clutter. Based on this model, the target scattering vector follows a KummerU PDF. Next, this PDF has been employed to derive an optimal segmentation algorithm based on the GLRT formalism. Results on synthetic and real data have shown that the proposed algorithm gives the best performances for the segmentation of high resolution data.

Références

[1] L. Bombrun and J.-M. Beaulieu. Fisher Distribution for Texture Modeling of Polarimetric SAR Data. *IEEE Geoscience and Remote Sensing*

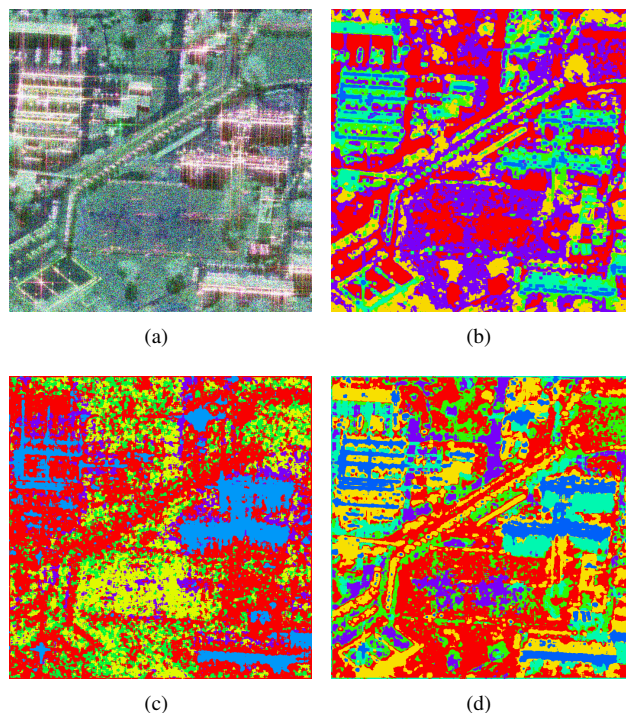


FIG. 3 – Classification results for the X-band RAMSES data over the Toulouse test-site (700×700 pixels) : (a) Colored composition of the target vector $[k]_1-[k]_3-[k]_2$, (b) Wishart criterion, (c) SIRV criterion, (d) KummerU criterion

Letters, 5(3), July 2008.

- [2] Y. Chitour, F. Pascal, P. Forster, and P. Larzabal. Exact maximum likelihood estimates for SIRV covariance matrix : Existence and algorithm analysis. *IEEE Transactions on Signal Processing*, 56(10) :4563–4573, 2008.
- [3] F. Gini and M. V. Greco. Covariance matrix estimation for CFAR detection in correlated heavy tailed clutter. *Signal Processing*, 82(12) :1847–1859, 2002.
- [4] M. S. Greco and F. Gini. Statistical analysis of high-resolution SAR ground clutter data. *IEEE Transactions on Geoscience and Remote Sensing*, 45(3) :566–575, 2007.
- [5] J.S. Lee, M.R. Grunes, T.L. Ainsworth, L.J. Du, D.L. Schuler, and S.R. Cloude. Unsupervised Classification Using Polarimetric Decomposition and the Complex Wishart Classifier. *IEEE Transactions on Geoscience and Remote Sensing*, 37(5) :2249–2258, 1999.
- [6] J.-M. Nicolas. Introduction aux Statistiques de Deuxième Espèce : Applications des Logs-moments et des Logs-cumulants à l'Analyse des Lois d'Images Radar. *Traitement du Signal*, 19(3) :139–167, 2002.
- [7] F. Pascal, Y. Chitour, J. P. Ovarlez, P. Forster, and P. Larzabal. Covariance structure maximum-likelihood estimates in compound Gaussian noise : existence and algorithm analysis. *IEEE Transactions on Signal Processing*, 56(1) :34–48, 2008.
- [8] F. Pascal, P. Forster, J. P. Ovarlez, and P. Larzabal. Performance analysis of covariance matrix estimates in impulsive noise. *IEEE Transactions on Signal Processing*, 56(6) :2206–2216, 2008.
- [9] H. L. VanTrees. *Detection, estimation, and modulation theory*. John-Wiley&Sons, New York, USA, 1968.
- [10] K. Yao. A representation theorem and its applications to spherically-invariant random processes. *IEEE Transactions on Information Theory*, 19(5) :600–608, 1973.